ISSN 1068-3356, Bulletin of the Lebedev Physics Institute, 2023, Vol. 50, No. 12, pp. 534–539. © Allerton Press, Inc., 2023.
Russian Text © The Author(s), 2023, published in Kratkie Soobshcheniya po Fizike, 2023, Vol. 50, No. 12, pp. 31–39.

Calibration and Reconstruction Algorithm for FARICH System of the Detector at Super Charm-Tau Factory

A. Yu. Barnyakov[a,d], V. S. Bobrovnikov[a], S. A. Kononov[a], P. D. Rogozhin[b], and M. V. Chadeeva[c,*]

[a] *Budker Institute of Nuclear Physics, Siberian Branch of the Russian Academy of Science, Novosibirsk, 630090 Russia*

[b] *Moscow Institute of Physics and Technology, Dolgoprudnyi, Moscow oblast, 141701 Russia*

[c] *Lebedev Physical Institute, Russian Academy of Sciences, Moscow, 119991 Russia*

[d] *Novosibirsk State Technical University, Novosibirsk, 630073 Russia*

**e-mail: chadeevamv@lebedev.ru*

Received July 30, 2023; revised October 18, 2023; accepted October 29, 2023

Abstract—To accomplish the physical program of studies at the planned Super Charm-Tau Factory electron-positron collider, a high-precision particle identification system is required. A FARICH–ring-imaging Cherenkov detector based on focusing aerogel and an array of silicon photomultipliers is proposed. The paper describes a reconstruction algorithm developed for such a detector. The algorithm was tested on simulated pion events with different photodetector noise levels. For dark count rates up to 10^5 Hz/mm^2, the factor β uncertainty is shown to be less than 5×10^{-4} (1×10^{-3}) for pions with momenta of 0.6–1.5 GeV/c and incident angles of 0°–10° (0°–45°) with respect to the normal to the detector plane.

Keywords: Cherenkov ring detector, silicon photomultiplier

DOI: 10.3103/S1068335623120047

1. INTRODUCTION

Experiments with electron–positron colliders are aimed at precision verification of the Standard Model and the search for new phenomena beyond it. Currently, the scientific community considers several versions of e^+e^--colliders of the next generation: the ILC in Japan [1], the CEPC in China [2], the CLIC and FCCee in CERN [3, 4]; in Russia, a project of an ultrahigh luminosity e^+e^- -collider ($\sim 10^{35}$ cm^{-2} s^{-1}) with a center-of-mass energy from 3 to 7 GeV, i.e., the Super Charm-Tau Factory (SCTF) is proposed [5]. The detector system for experiments on the SCTF collider has a standard cylindrical structure with a track detector, a particle identification system, an electromagnetic calorimeter, and a muon detector. To solve the physical problems, in particular for studying rare decay modes of charmed mesons, the search for CP violations and lepton flavor violation in taulepton decays, particle identification system is required, which can provide reliable separation of electrons, muons, pions, and kaons in the momentum range of 0.5–1.5 GeV/c [6]. For example, to separate muons and pions at the level of three standard deviations, the factor β measurement accuracy should be no worse than 0.005 (0.0006) for pion momenta 0.5 (1.5) GeV/c.

The paper presents the developed algorithm for searching the Cherenkov signal and estimating the factor β for the identification system based on focusing aerogel with Cherenkov radiation detection by arrays of silicon photomultipliers (SiPMs) [7]. Tests on simulated events took into account also a possible increase in noises caused by SiPM radiation damages [8]. The proposed method allows for a required β measurement accuracy (at the level better than 10^{-3}) up to the photodetector noise level expected after several years of SCTF operation.

2. PROJECT AND MODEL OF THE CHERENKOV RING DETECTOR FOR THE SCTF

The particle identification system in the detector at the SCTF will be placed between the track chamber and electromagnetic calorimeter. The Cherenkov detector based on focusing aerogel (FARICH) makes it possible to improve the measurement accuracy of the particle velocity due to a decrease in the Cherenkov ring width because of the variable refractive index of aerogel [7].

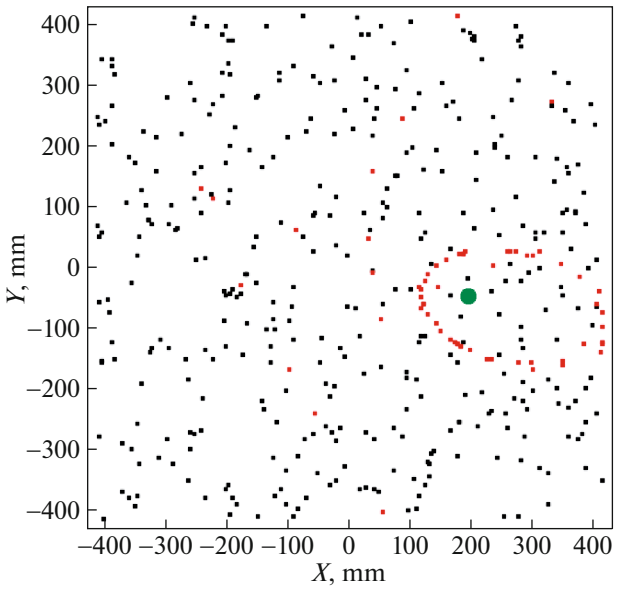

Fig. 1. Example of the Cherenkov signal (red squares) from the pion with parameters $\beta = 0.998$ and $\theta_p = 45°$. The green circle means the intersection of the Cherenkov cone axis with the photodetector plane. Closed squares correspond to noise hits at DCR = 10^5 Hz/mm^2.

In this study, the results are presented of simulation of a similar system with a photodetector area of 830 × 830 mm^2 without magnetic field using the Geant4 package tools [9].

In the FARICH prototype model under consideration, a radiator consists of four aerogel layers 9.32, 8.93, 8.55, and 8.20 mm thick with refractive indices of 1.041, 1.044, 1.047, and 1.050 (in the direction toward the photodetector). At a distance of 200 mm from the radiator and in parallel to it, a layer of photodetectors composed of 900 square arrays of silicon photomultipliers with spacings between them of 1 mm is arranged.

The number of SiPMs in the array is 8 × 8, the surface area of each SiPM is 3.16 × 3.16 mm^2. In such a configuration, the total number of SiPMs is 56700, and the sensitive area fraction (space factor) is 82%.

In the simulation, the source of single charged pions was placed at a distance of 1 mm from the radiator, and pion factors β were uniformly distributed in the range of 0.957–0.999. The emission angles θ_p of primary particles with respect to the normal to the photodetector plane varied in the range of 0–45° with a uniform distribution over the cosine of this angle. In addition to the simulation of the ionization loss and Cherenkov radiation generation, the Geant4 package methods for optical photon transport allow the consideration of optical properties of materials. The simulation was also complemented by detector effects, i.e., the time resolution of electronics (200 ps), the signal readout time interval (20 ns), and the SiPM efficiency (of the order of 38% at the maximum Cherenkov radiation wavelength of 400 nm).

The event simulation results are hits, i.e., SiPM signals recorded in the binary mode, i.e., without analysis of the signal amplitude and the number of photons simultaneously arrived at the same pixel.

In this mode, the correlated noises of SiPMs themselves do not affect the number and spatial distribution of hits. In addition to the case of ideal photodetectors, version of addition of SiPM noise hits up to the dark count rate (DCR) of 10^6 Hz/mm^2 were analyzed (see the event example in Fig. 1). For each hit, the data is saved on its measurement time with respect to the time point of the primary particle generation. In the detector configuration under consideration taking into account the time resolution, the variance of photon detection times in one event is on average 1 ns.

3. RECONSTRUCTION METHOD

The main task is the determination of the factor β of a particle by the projection of the Cherenkov ring to the photodetector plane. The measurement result is affected by ring spreading due to the thickness of the aerogel layer in which Cherenkov radiation is generated, the size of an individual SiPM, the Cherenkov

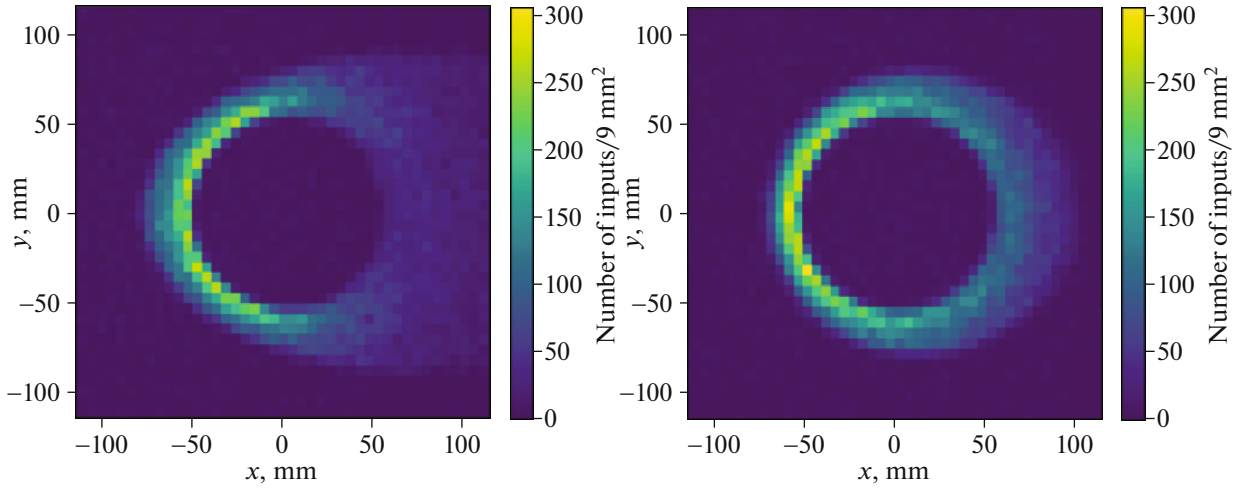

Fig. 2. Signal from Cherenkov photons before (left) and after (right) rotation of the virtual plane of photodetectors with respect to the Cherenkov cone axis ($x = 0$ mm, $y = 0$ mm) for pions with factors $0.990 \le \beta \le 0.999$.

angle scatter because of the chromatic dispersion of the aerogel refractive index, the elliptic shape of the Cherenkov cone section, and the variance of the photon times of flight due to the particle trajectory inclination with respect to the photodetector plane, as well as the ellipse shape distortion due to refraction at the aerogel–air interface, which depends on the photon emission angle. The reconstruction procedure includes several stages.

3.1. Geometrical Transformations and Time of Flight Correction

In the simulation, the primary particle momentum direction is set in the generator; in a real experiment, the momentum will be measured in the track detector. The intersection point of the Cherenkov cone axis with the photodetector plane (OXY) is determined by the direction of the primary particle momentum. The larger the angle between the direction of the primary particle and the normal to the photodetector plane, stronger the distortion of the recorded Cherenkov ring. To reduce these distortions, it is necessary to pass to the virtual plane perpendicular to the Cherenkov cone axis. The rotation also includes a correction of relative times of photon detection, which can reach several hundred picoseconds for maximum angles. The simulation conditions control the maximum expected ring size, which makes it possible to limit the search area of the signal cluster 400×400 mm^2 in size with a center at the point OXY. Figure 2 shows the example of the arrangement of signal hits in the photodetector coordinate plane (x, y) before and after geometrical transformations.

3.2. Search for the Signal Cluster

In the (r,ϕ) coordinates, where r is the distance from the SiPM with a hit to the point OXY, and ϕ is the azimuthal angle in the turned photodetector plane, the signal shape is a wave. Then integration over the azimuthal angle and the transformation to the coordinates (r,t) is performed, where t is the pixel response time. The consideration of the hit time improves the reconstruction quality in the noise conditions. An example of the two-dimensional histogram with the number of hits $N(r,t)$ in one event is shown in Fig. 3. The next algorithm step is the search for a signal cluster, i.e., the (r_0,t_0) coordinates corresponding to a maximum of $N(r,t)/r$, since the number of hits in the ring is approximately proportional to its radius. In the factor β range under study, the number of triggered pixels in the event is from several units to several tens. The maximum was searched by scanning with step δr and sliding window width Δr along r coordinate and with step δt and sliding window width Δt along t coordinate. To take into account the distortions due to the particle trajectory inclination and refractions on the aerogel boundary, the recon-

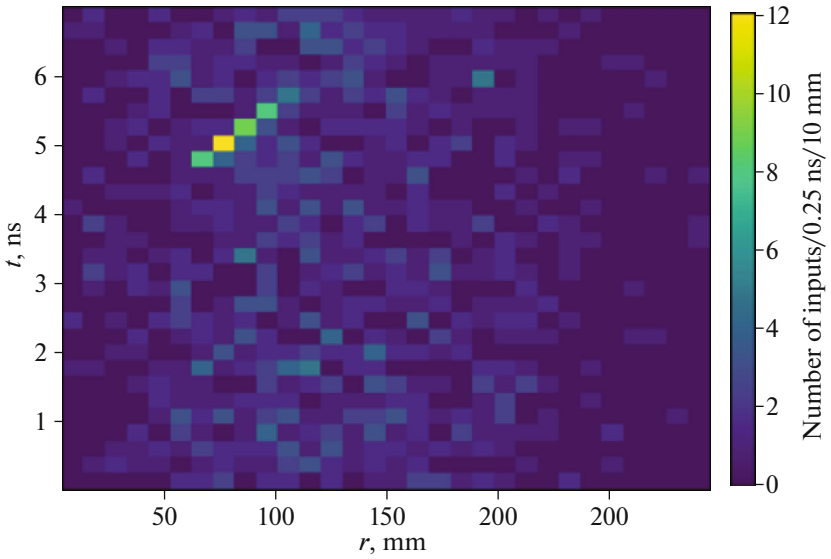

Fig. 3. Example of the joint distribution of hit recording times (t) and distances (r) to the Cherenkov cone axis for the pion with parameters $\beta_{true} = 0.998$, $\theta_p = 45°$ (DCR = 10^6 Hz/mm^2).

structed radius R_{reco} is calculated as a weighted average in the range of $\pm n$ scanning steps over r and $\pm m$ scanning steps over t using the following expressions

$$w_i = \frac{\sum_{j=-m}^{m} N(r_i, t_j)}{2m+1}, \quad R_{reco} = \frac{\sum_{i=-n}^{n} w_i \cdot r_i}{\sum_{i=-n}^{n} w_i}, \tag{1}$$

where $r_i = r_0 + i \cdot \delta r (-n \le i \le n)$, $t_j = t_0 + j \cdot \delta t (-m \le j \le m)$.

3.3. Calibration and Optimization of Parameters

In the general case, the reconstructed radius differs from the ideal radius corresponding to the true factor β_{true}. In the algorithm under study, the desired value of β_{reco} is obtained from the calibration dependence $\beta_{true}(R_{reco}, \theta_p)$. The values of β_{true} are accessible in the simulation at the generator level and in experiments with test beams when testing prototypes. Figure 4 shows the example of the projection of the calibration dependence onto the plane (β_{true}, R_{reco}). The dependence $\beta_{true}(R_{reco}, \theta_p)$ was approximated using the Gauss function with logarithmic transformation and parametrization of angular dependences,

$$\ln \beta = \ln f_1(c) - \left(\frac{R_{reco} - f_2(c)}{f_3(c)} \right)^2, \quad f_i(c) = a_{0i} + a_{1i} c + a_{2i} c^2, \quad c = \cos \theta_p. \tag{2}$$

The approximation by the unbinned maximum likelihood method yields nine calibration factors a_{ki}, after which the values of β_{reco} are calculated in each event by the known angle θ_p and the reconstructed radius β_{reco} using expression (2). An estimate of the reconstruction accuracy is the distribution width of the difference $\Delta\beta = RMS_{90}(\beta_{reco} - \beta_{true})$, where 90% of the sample around the average to exclude outliers are used to calculate the root-mean-square RMS_{90}.

The scanning (Δr, δr, Δt, and δt) and averaging (n and m) parameters were optimized by exhaustive search method and comparison of the reconstruction accuracy $\Delta\beta$ at various noise levels at a sample of 200000 events. The best accuracy was obtained at the following values: $\Delta r = 6$ mm, $\delta r = 3$ mm, $\Delta t = 0.25$ ns, $\delta t = 0.25$ ns, $n = 4$, and $m = 4$.

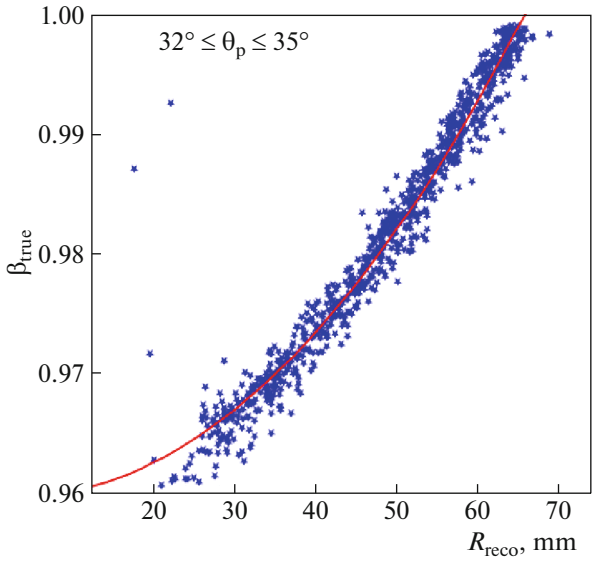

Fig. 4. Blue symbols are projections of the two-dimensional dependence $\beta_{true}(R_{reco}, \theta_p)$ for primary particle emission angles $32° \le \theta_p \le 35°$; red curve is the Gaussian approximation.

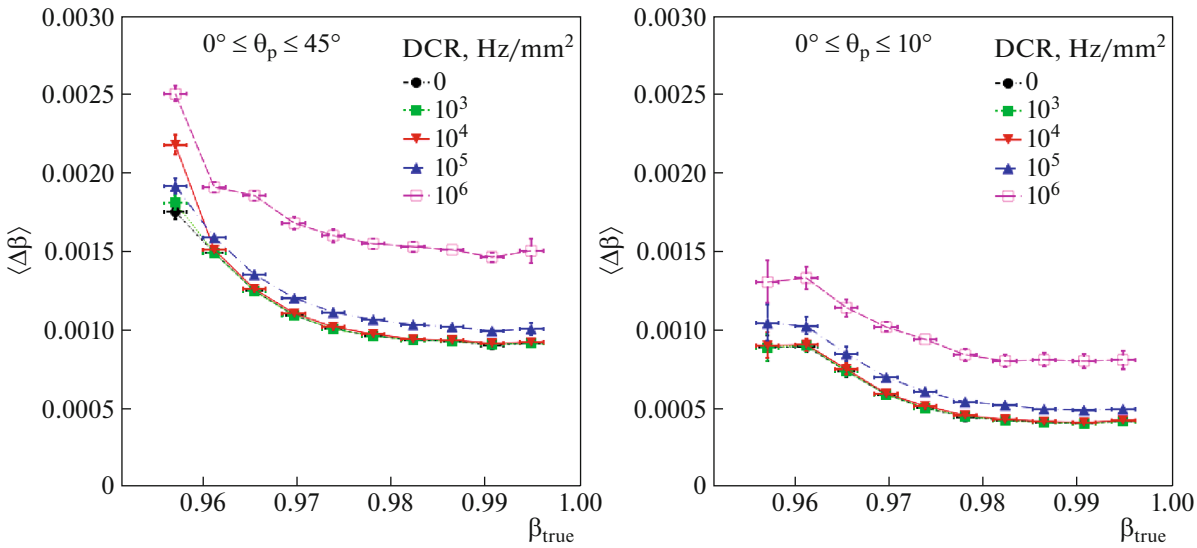

Fig. 5. Dependence of the factor β reconstruction accuracy on the true value β_{true} for various dark count rates of photodetectors (DCR) at primary particle emission angles 0°–45° (left) and 0°–10° (right). See text for details.

4. RESULTS

To estimate the algorithm accuracy by the cross-validation method, a complete set of 1200000 simulated events was divided into 10 equal parts, which were used independently to obtain calibration factors at optimum parameters (see Section 3). Each set of factors was applied to the complete sample to determine the values of $\Delta\beta_k$ $(1 \le k \le 10)$ in the ranges of β_{true}. As a final estimate of the reconstruction accuracy, the average value $\langle\Delta\beta\rangle = (\sum_{k=1}^{10}\Delta\beta_k)/10$ was taken in each β_{true} range; as a systematic uncertainty, the root-mean-square of this average was taken. Similarly, the accuracy in the case of adding photodetector noises was determined. Figure 5 (left) shows the dependence of the reconstruction accuracy of the factor β on the true factor β_{true} for the pions emitted at angles from 0° to 45° with respect to the normal to the plane of photodetectors at various dark count rates. Error bars show the systematic uncertainty obtained by the cross-validation method, which exceeds the statistical uncertainty by an order of magnitude.

At additional constraints to the pion emission angle (to 10°) and to the number of signal hits (no less than 5), the measurement uncertainty decreases by half (Fig. 5 right).

The algorithm performance depends on the primary particle momentum direction with respect to the photodetector plane, on the true factor β_{true} (defining the Cherenkov ring size) and the photodetector noise level. For factors $\beta_{true} < 0.97$, the algorithm accuracy corresponds to the requirements imposed on the FARICH detector at all studied noise levels. For the range of $0.97 \le \beta_{true} \le 0.999$, the developed algorithm provides the reconstruction accuracy no worse than 5×10^{-4} (1×10^{-3}) at emission angles to 10° (45°) and shows the stability up to noises of 10^5 Hz/mm^2. An increase in the uncertainty up to ~ 0.0016 occurs as the dark count rate increases to 10^6 Hz/mm^2. An additional contribution to the systematic uncertainty can be expected for the case of incomplete Cherenkov rings, when the primary particle trajectory is close to the detector edge.

One of the possible methods of further accuracy improvement is the implementation of machine learning methods in the reconstruction algorithm.

ACKNOWLEDGMENTS

The software package for creating the digital model of the FARICH detector used in this study, is developed within the scientific program of the National Center of Physics and Mathematics, direction no. 6 "Nuclear and radiation physics."

FUNDING

This work was supported by ongoing institutional funding. No additional grants to carry out or direct this particular research were obtained.

CONFLICT OF INTEREST

The authors of this work declare that they have no conflicts of interest.

REFERENCES

1. Yamamoto, H., The international linear collider project—Its physics and status, *Symmetry*, 2021, vol. 13, no. 4, pp. 674–689. https://doi.org/10.3390/sym13040674
2. Gao, J., CEPC and SppC status–From the completion of CDR towards TDR, *Int. J. Mod. Phys. A*, 2021, vol. 36, no. 22, pp. 2142005. https://doi.org/10.1142/S0217751X21420057
3. Franceschini, R., Beyond the standard model physics at CLIC, *Int. J. Mod. Phys. A*, 2020, vol. 35, no. 15, p. 2041015. https://doi.org/10.1142/S0217751X20410158
4. Abada, A. (FCC Collab.), FCC physics opportunities: future circular collider conceptual design report volume 1, *Eur. Phys. J. C*, 2019, vol. 79, no. 6, pp. 474–635. https://doi.org/10.1140/epjc/s10052-019-6904-3
5. Bondar, A.E., (Charm-Tau Factory Collab.), Project of a Super Charm-Tau factory at the Budker Institute of Nuclear Physics in Novosibirsk, *Phys. Atom. Nucl.*, 2013, vol. 76, pp. 1072–1085. https://doi.org/10.1134/S1063778813090032
6. Achasov, M.N. (SCTF Collab.), Super Charm-Tau Factory: Physics programme (2022). https://sct.inp.nsk.su
7. Barnyakov, A.Yu., Barnyakov, M.Yu., Bobrovnikov, V.S., Buzykaev, A.R., Daniluyk, A.F., Duren, M., Hayrapetyan, A., Katcin, A.A., Kayan, H., Kononov, S.A., Kravchenko, E.A., Kuyanov, I.A., Ovtin, I.O., Podgornov, N.A., Pomuleva, S.I., et al., Progress and perspectives of FARICH R&D for the Super Charm-Tau Factory project, *Nucl. Instrum. Meth. A*, 2022, vol. 1039, p. 167044. https://doi.org/10.1016/j.nima.2022.167044
8. Calvi, M., Carniti, P., Gotti, C., Matteuzzi, C., and Pessina, G., Single photon detection with SiPMs irradiated up to 10^{14} cm^{-2} 1-MeV-equivalent neutron fluence, *Nucl. Instrum. Meth. A*, 2019, vol. 922, pp. 243–249. https://doi.org/10.1016/j.nima.2019.01.013
9. Allison, J. (Geant4 Collab.), Recent developments in Geant4, *Nucl. Instrum. Meth. A*, 2016, vol. 835, pp. 186–225. https://doi.org/10.1016/j.nima.2016.06.125

Translated by A. Kazantsev

Publisher's Note. Allerton Press remains neutral with regard to jurisdictional claims in published maps and institutional affiliations.